IEEE Transactions on Field Robotics (T-FR) paper, presented at ICRA 2026, Vienna, Austria. Cite as T-FR paper.
IEEE Transactions on Field Robotics
Special Issue on Space Robotics

Received 21 February 2025; revised 7 August 2025; accepted 16 September 2025.
Date of publication 22 September 2025; date of current version 10 October 2025.
This article was recommended by Executive Editor Teresa Vidal-Calleja.

Digital Object Identifier 10.1109/TFR.2025.3612365

Steerable High-Jumping Tensegrity Robot for Space Exploration

JONATHAN JACOB KOLT GREEN, DARIO BOZINOVSKI, FABIAN TISCHHAUSER, MARCO HUTTER, (Member, IEEE), AND ROBERT BAINES, (Member, IEEE)

ETH Zurich, 8092 Zurich, Switzerland

CORRESPONDING AUTHOR: ROBERT BAINES (rbaines@ethz.ch)

This work was supported by the Branco Weiss Fellowship–Society in Science, Administered by ETH Zurich.

This article has supplementary downloadable material available at https://doi.org/10.1109/TFR.2025.3612365, provided by the authors.
(Regular Article)

ABSTRACT The growing interest in exploring other planets calls for innovative robotic systems capable of deploying to and traversing challenging space environments. While wheeled rovers have traditionally fulfilled this role, they face limitations, including configuration dependence (e.g., requiring an upright orientation), susceptibility to impacts, and difficulty overcoming obstacles larger than their wheel radius. Tensegrity-based robotics presents a promising alternative for future rovers. These lightweight, compliant structures offer compactibility, adjustable stiffness, and the ability to absorb impacts without damage. Moreover, their unique form factor naturally protects scientific payloads. Recent research has explored tensegrity robots for rolling-based locomotion, with increasing interest in leveraging their structures for jumping-based movement. However, achieving hardware capable of high jumps greater than the robot's body length (BL) and directional jumping control for steerable jumping remains a challenge. This work introduces a tensegrity robot that utilizes structural deformation for jumping locomotion. Through first-principles analyses, simulations, laboratory experiments, and field tests in a planetary analog environment, we demonstrate a robot capable of vertical jumps of 1.18 m (1.93 BLs), directional jumps covering horizontal distances up to 0.59 m (0.97 BLs), and surviving falls from heights of 21.5 m (35.2 BLs). The robot can also reduce its occupied volume by more than 4× without sustaining damage. Results herein highlight the potential of jumping tensegrity robots as robust, versatile platforms for next-generation space exploration.

INDEX TERMS Jumping locomotion, mechanisms, space robotics, tensegrity robotics.

I. INTRODUCTION

AS HUMANITY sets its sights on new frontiers in space—exploring the Moon, asteroids, and other planets for resource acquisition and potential human settlement—the demand for advanced robotics that reliably deploy to and locomote in challenging environments increases [4], [12], [25]. Most robotic systems successfully deployed on extraterrestrial surfaces have been wheeled rovers [21]. Despite their pivotal scientific role, wheeled rovers suffer from a number of shortcomings that impede their application to upcoming space exploration scenarios [41]. These shortcomings can broadly be sorted into those concerning robotics: 1) deployability and 2) mobility.

From the perspective of deployability, wheeled systems generally operate effectively only when in a particular configuration relative to the ground (i.e., ''upright''). Furthermore, most wheeled rovers are unable to withstand high impacts, such as in a scenario where dedicated airbags, lander thrusters, or equipped parachutes fail during the robot's descent to the surface. Recent lunar lander accidents underscore how orientation dependence and vulnerability to impact can jeopardize expensive scientific missions: intuitive machines' IM-1 tipped over and lost functionality upon touchdown [7], while SpaceIL's Beresheet was destroyed upon crashing into the Moon's surface [14].

In terms of mobility, wheeled robotic platforms struggle to traverse obstacles much larger than their wheel radius [35]. Scientific features of interest on the Moon and Mars, such as cliffs, ridges, crater rims, and lava tubes, exhibit protruding rock features as large as several meters [16], [32]. Overall,

the uncertainties posed by unstructured terrain force mission planners to explicitly avoid rugged patches and terrain discontinuities, despite these being areas of great scientific import [15], [30].

The past decade has witnessed the rise of a new prospect for space rovers that has the potential to address the deployability and mobility shortcomings of standard wheeled platforms: the tensegrity robot. Tensegrity robots are composed of rigid struts held in a compressed equilibrium configuration by a network of tensioned cables [20], [24]. The absence of bending moments and radial forces within the structure minimizes mass while providing high resistance to impact damage [9]. Such resistance is achieved by eliminating rigid interfaces between the structure's struts, which effectively mitigates the formation of large stress concentrations [27], [37]. Due to tensegrity robots' high compliance, deformation capability, and impact damage resistance, they could one day be deployed to extraterrestrial bodies without a dedicated landing system to slow their descent through the atmosphere, as well as survive routine impacts occurring when traversing cliffs and ridges [5]. Although the inherent properties of the tensegrity paradigm offer a clear way to enhance rover deployability, its potential to improve rover mobility amid rugged terrains remains less well-investigated.

Among tensegrity locomotion strategies such as vibration, swimming, flying, and crawling [29], state-of-the-art tensegrity systems, such as NASA's SUPERball v2, normally engage in punctuated rolling. During punctuated rolling, a robot repeatedly shifts its center of mass (CoM) to tip onto a desired face [39]. Punctuated rolling is typically slow (on the order of a few body lengths (BL) per minute, energetically costly (the robot must deform by a large amount for each notable translation of its center of mass), and ill-suited to unstructured terrain. Geological formations many times larger than the robot's body, as well as steep inclines, together pose insurmountable features for punctuated rolling.

There has also been a fair body of research seeking to address the challenges of tensegrity mobility over difficult terrains via control. Using genetic algorithms [26] or deep reinforcement learning [40] in simulation, researchers converged on tensegrity gaits capable of moving in arbitrary directions [34], up inclines [8], and over obstacles a fraction of the robot's BL [36]. Confined mainly to simulation, these works did not showcase hardware capable of overcoming obstacles larger than the tensegrity's body.

Jumping is an alternative locomotion mode to punctuated rolling that offers to improve speed, enable circumventing large obstacles, and increase the robot's capability to traverse unstructured terrain. The benefits of jumping scale favorably as gravity decreases: a jumping robot will travel higher and further laterally with the same amount of energy released in lower gravity. In contrast, punctuated rolling does not markedly increase in efficacy when gravity is lower, since this locomotion mode requires the robot to repeatedly displace its CoM orthogonal to gravity.

Jumping tensegrity systems have been demonstrated that employ additional thrusters [19], propellers [22], [28], and highly dynamic actuators that impact against the ground [17]. Utilizing the tensegrity structure of the robot itself to store and release energy for jumping has the potential to simplify the robot by uniting the actuators dedicated to jumping, nominal locomotion, and shape change. For instance, in [10], jumps were demonstrated by actuating a tensegrity structure made from shape-memory alloy springs, but these jumps did not exceed a height of 0.98 BL. Moreover, the work did not demonstrate control over the direction of the jump. A high-jumping (defined here as >1 BL) tensegrity robot was proposed in [13]; however, high jumping was demonstrated only in simulation.

In summary, no work to date has realized and characterized a tensegrity robot capable of controllable directional jumps and vertical high jumping using its own structure. In this work, we

1) introduce a clutch-based actuation strategy that leverages tensegrity deformations for jumping and enables vertical jumps of 1.18 m (1.93 BL) [Fig. 1(a)];
2) investigate directional control of jumps through varied cable tensions [Fig. 1(b)];
3) validate configuration-invariant jumping and robot mechanics using physics-based simulations;
4) demonstrate the robot's ability to withstand impacts from heights of 21.5 m (35.2 BL) and maintain functionality in unstructured, extraterrestrial-analog terrain [Fig. 1(c) and (d)].

Overall, this work combines structural design, actuation, and a dynamic locomotion approach to set a new standard for jumping tensegrity performance. The results discussed herein broadly reveal design considerations and mechanical phenomena associated with jumping tensegrity robots harnessing the deformation of their structures and suggest they are promising candidates for future space rovers. A comparison of the presently considered system with existing tensegrity robots is available in Appendix A in the supplementary material.

II. SYSTEM DESIGN

A. OVERVIEW

The jumping tensegrity robot [Fig. 2(a)] is composed of six identical strut assemblies (500-mm-long carbon fiber-reinforced polymer tubes). The struts were selected to withstand axial impact loads as high as 650 N (see Appendix B in the supplementary material for further explanation and justification for the strut choice). The struts are suspended in a network of 24 cables. Both ends of each strut mate with a node assembly that serves to connect the cables and struts and protect the end of the strut [Fig. 2(b)]. The node assemblies consist of two 3-D printed parts. The hub (gray) is made from polylactic acid (PLA) and attaches to cables via small screw clamps. The endcap (red) is fabricated out of a flexible thermoplastic polyurethane (TPU).

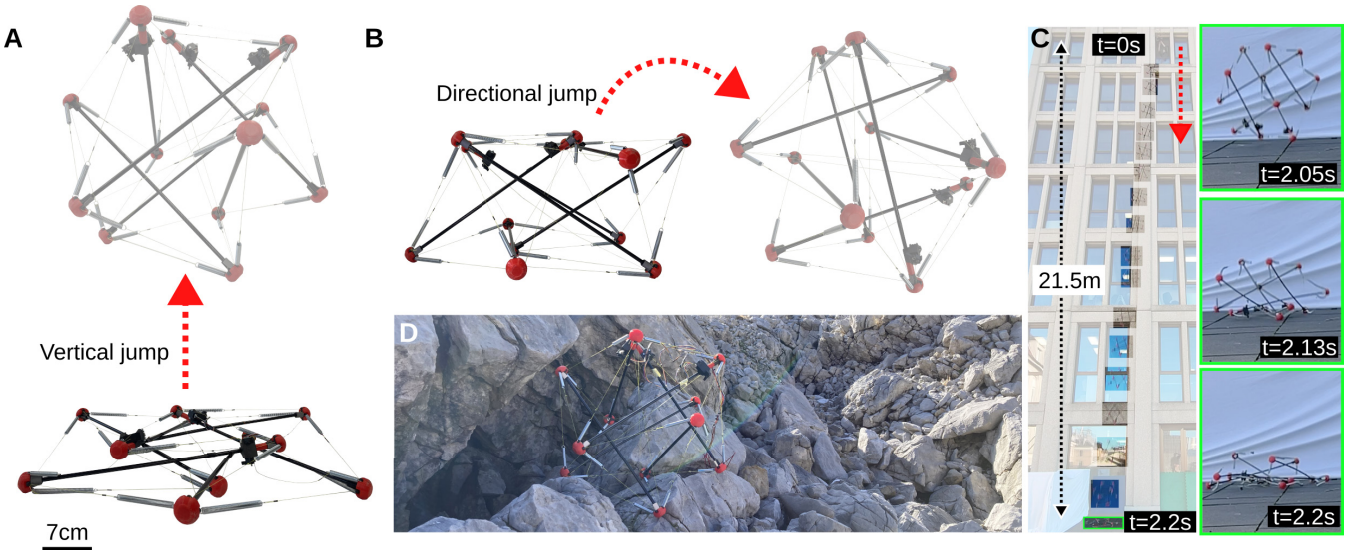

FIGURE 1. Directional high-jumping tensegrity robot. (a) Vertical jumping is accomplished by uniformly compressing the structure. (b) Varying the degree of tension in each of the three actuators permits directional jumping. (c) Robot structure withstands multiple drops from 21.5-m heights onto concrete. Inset images contoured in green show freeze frames during the impact with the ground, in which the tensegrity robot experiences a high degree of global structural deformation. (d) Robot can locomote and survive impacts on rugged terrain.

Each structural cable contains an elastic spring section (410-N/m galvanized piano wire spring) and an inelastic cable section (0.29-mm diameter ultrahigh-molecular-weight polyethylene braided cable, rated for a maximum load of 259 N). The structural cables are preloaded to a tension of 12.5 N to equilibrate the robot to a six-bar icosahedron topology [10], [17], [19], [22], [38], [39]. We chose a six-bar icosahedron for the form of the tensegrity robot because it is the minimal structure that is symmetric about three orthogonal axes, highly deformable, and closely approximates a sphere, making it apt for distributing impact loads and landing on and jumping from any configuration.

Three actuators are mounted on the tensegrity's struts that apply tension to inelastic actuator cables, globally deforming the tensegrity to store energy for jumping. We arranged the actuators and actuator cables in a "skew-central" actuation topology spanning the diagonally opposite points in each pair of parallel struts [visualized as the three yellow cables in Fig. 2(a)]. Although there are many potential ways to realize the actuation topology, the skew-central configuration permits a high degree of control over the robot's structure, unlocking the ability to elicit large deformations that uniformly flatten the robot for vertical high jumping, as well as asymmetrically deform the robot for directional jumping by superpositioning different levels of tension in each of the three actuators. Having only three actuators also reduces the robot's mass compared to conventional tensegrity robot actuation topologies that use one actuator per structural cable.

Many tensegrity robots have actuators mounted at the ends of their struts [11], [39], but the present robot design incorporates actuators housed within the bounding polyhedron of the tensegrity to protect them. The actuators are mounted to the struts using sliding collars, which mechanically decouple them from the structure along the axis of cable tension [Fig. 2(b)]. If a cable experiences a sudden high force, such as that caused by an impact, the actuator is free to translate along the strut and avoid directly transmitting the force to the relatively fragile actuators. While such sliding collars add a degree of mechanical complexity to the robot and could potentially be jammed by environmental obstacles, we opted to prioritize the impact resistance capability to support safer jumping.

In the robot's rest state, the actuator cables are slightly slack. Preparing for a jump, the actuator reels in the cable, removing the slack. The actuator slides upward along the strut until it contacts a compliant bumper made of TPU. At this point, the actuator unit couples to the tensegrity structure such that it can exert tension on the cables in preparation for a jump. Upon jumping, the actuator decouples from the structure and remains decoupled during subsequent impacts. This arrangement helps mitigate potentially damaging vibrations and impulse loads propagating through the actuators upon landing.

The fully assembled robot has a mass of 507 g and a volume of 0.119 m^3 (nominal, unactuated). The resulting density, 4.26 kgm^{-3}, is even lower than common packaging foam [3]. A tether runs from the robot to an external power supply and computer. See Appendix D in the supplementary material for a more detailed breakdown of the robot and its components.

B. ACTUATOR DESIGN

We created a custom actuator unit to deform the tensegrity structure to store energy for jumping. The actuator contains a combined winch and clutch mechanism, inspired by active clutch designs [18] [Fig. 2(c)]. This mechanism unites

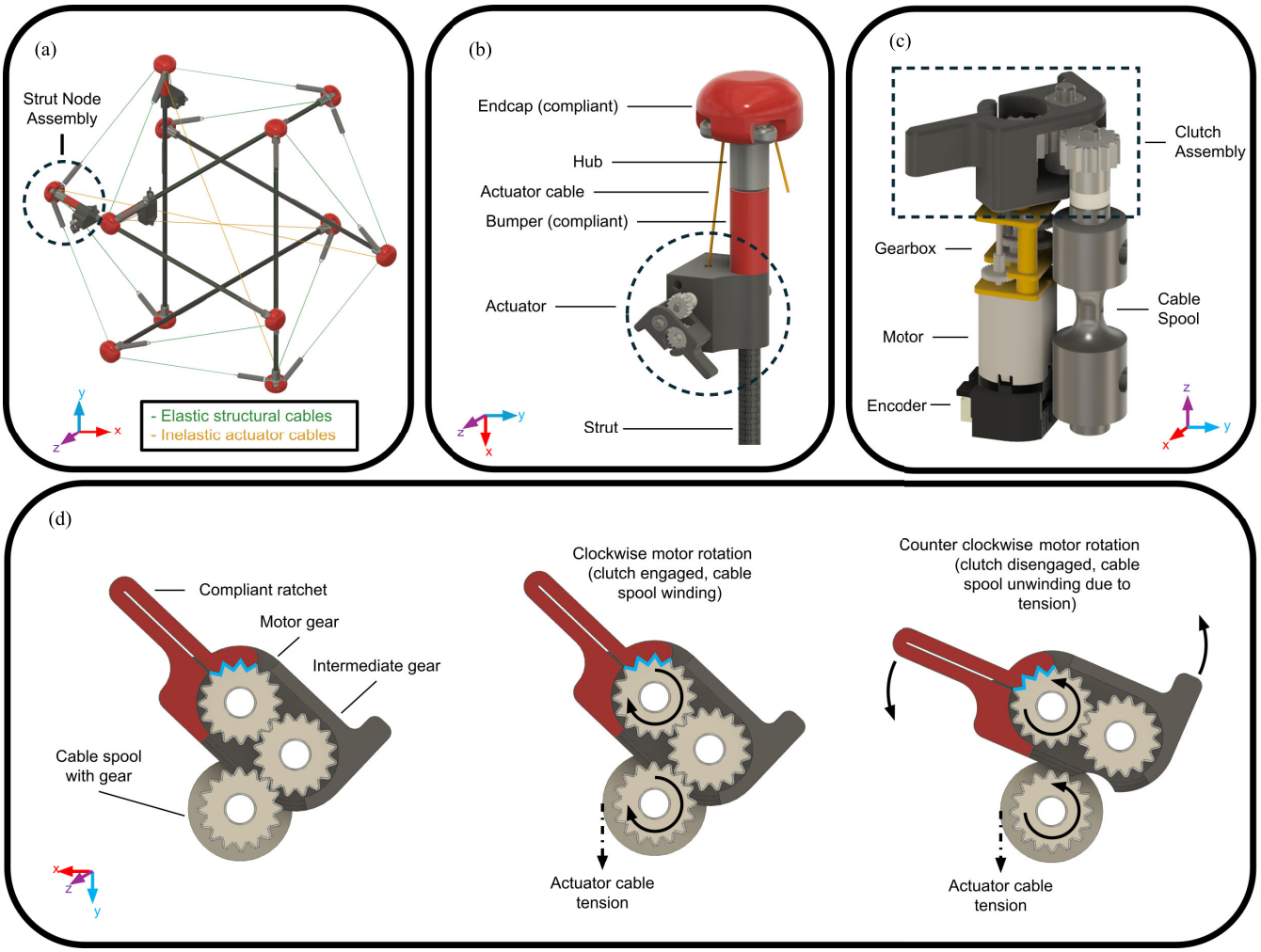

FIGURE 2. Design of the jumping tensegrity robot. (a) CAD model of robot featuring strut assemblies, structural cables, actuator cables, and actuators. (b) Strut node assembly protects compliant elements, routing for the actuator cable, and attachment points for the structural cables and springs on the hub. (c) Components of an actuator (the protective case has been removed to show the internal components). (d) Clutch mechanism components illustration (for increased visibility, the compliant ratchet is colored red and the engaged ratchet tooth is colored blue).

functionalities for winch winding, clutch engagement, and clutch disengagement and only uses a single motor.

The actuator unit comprises a three-piece gear train that links a motor (Pololu 5228) to a cable spool. Both the motor's drive gear and an intermediate gear are mounted in the clutch module, and the entire clutch module can pivot about the motor shaft. The third gear is attached to a spool around which the inelastic actuator is wound. The spool sits tightly within a housing [circled in Fig. 2(b)] to ensure that the cable is constrained and cannot unravel or tangle when it is slack.

When the motor rotates clockwise, the clutch engages and the winch winds at a constant rate. A quadrature encoder is attached to the motor shaft to estimate the change in cable length. The motor can then be rotated counterclockwise, which will engage the ratchet and cause the clutch to pivot. The clutch pivoting disengages the intermediate gear, allowing the winch to freely unwind, releasing the tension on the actuator cable [Fig. 2(d)]; Supplementary Video). Due to the high gear reduction ratio (986:1) on the output of the motor, the mechanism is not back-drivable. Thus, the robot can maintain any deformed state after tensioning the cables without power.

III. ROBOT CHARACTERIZATION

We conducted an array of simulations and hardware experiments on the robot to assess its vertical and directional jumping, self-righting by rolling, robustness to impacts, and shape changing—key performance considerations for space applications. Furthermore, we sought to gain insights into the governing physical principles and actuation strategies for this new type of tensegrity robot. We used the NASA Tensegrity Robotics Toolkit (NTRT) to simulate the robot [23] (see Appendix G in the supplementary material for more information about the simulation setup).

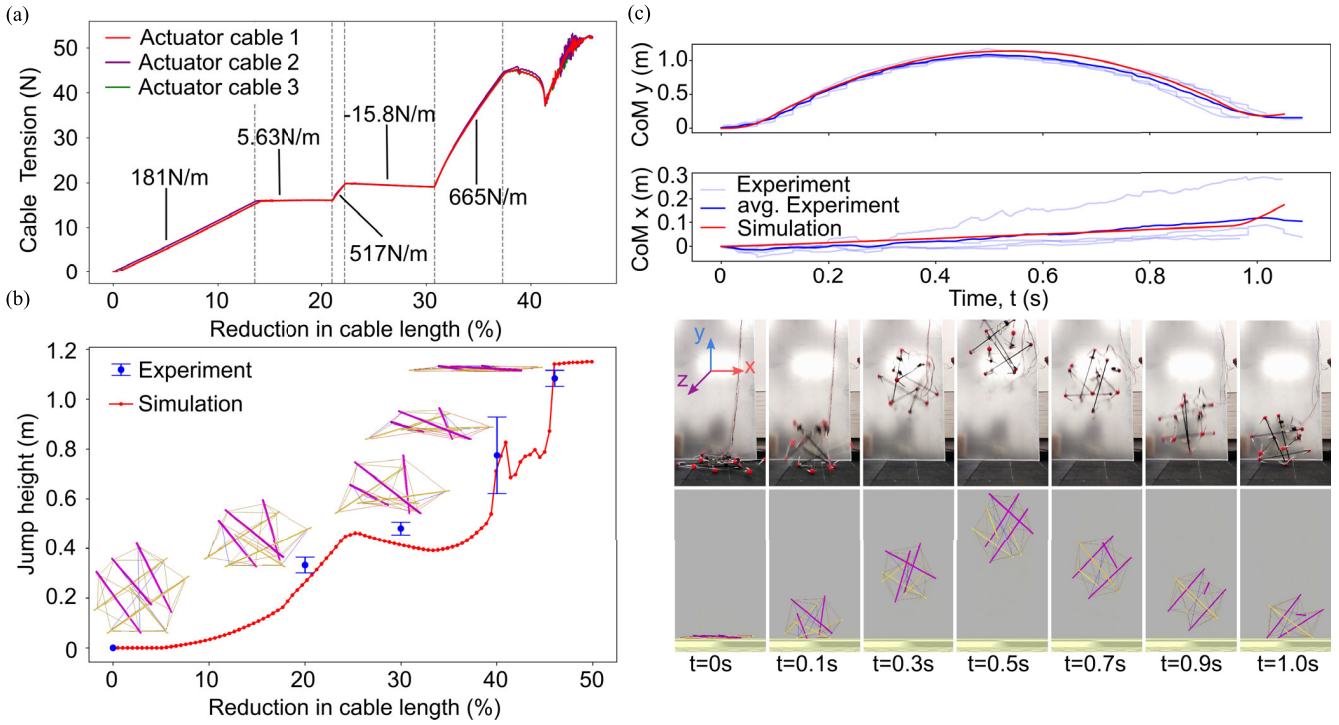

FIGURE 3. Vertical jumping characterization. (a) Simulation of tension in the cables as a function of reduction in cable length. The regions of different slopes correspond to different global stiffness modes of the structure. (b) Influence of reduction in cable length on resulting jump height, including simulated and real data points. Inset simulation snapshots illustrate the robot's global structural compression at the given data point. Error bars indicate one standard deviation from the mean over four trials. Maximum jump height is achieved by compressing the tensegrity all the way to its flat configuration, storing the largest amount of elastic energy. (c) Comparison between simulated and experimental vertical jumps, tracking vertical (*y*) and horizontal (*x*) movement of the robot's center of mass.

A. VERTICAL JUMPING

Vertical jumps are achieved by tensioning all three actuator cables equally, resulting in symmetric flattening of the tensegrity robot. To understand the forces and elastic energy stored in the structure during jumping, we conducted simulations to estimate the relationship between changes in actuator cable length and the resulting tension. All cables were tensioned simultaneously by the same amount, up to a 50% reduction in length.

Simulation results reveal that tensioning the robot elicits distinct stiffness regimes in the cables [Fig. 3(a)]. Since the skew-central actuation topology overconstrains the structure, we observe sharp transitions between different forms with different stiffnesses as the robot compresses, producing the piecewise affine sections of the plot. The nonlinear regime transition beginning at approximately 38% reduction in cable length is where the structure collapses into a flat configuration. The downward-sloped curved section is where the structure "pulls" itself into a stable flat configuration. The noisy, broadly increasing region of the plot that closely follows arises from self-collisions when trying to further deform the structure once it is already flat.

Integrating the tension over the actuator cable's length change yields the energy stored in the structure, serving as a proxy for jump height. The rate of energy storage through structural deformation increases with higher actuator cable tensions (see Appendix E in the supplementary material). Practically, this means that achieving incremental additional jump height requires significantly greater actuator tensions. On the actual robot, motor displacement is measured using encoders, allowing inference of global tension as a function of motor position and enabling open-loop control of vertical jump height.

To more directly analyze the effect of actuator cable length reductions on jump height, we performed both simulations and experiments on the physical robot. Cable lengths were commanded to reduce by 20%, 30%, 40%, and 46%, and the resulting jump heights were measured. On the physical robot, we conducted four jumps for each reduction level. Data were collected by tracking the trajectories of the robot's endcaps using slow-motion footage. These trajectories were averaged to estimate the centroid path, from which jump height was calculated (see Appendix H in the supplementary material).

At a 46% reduction in actuator cable length, corresponding to a tension of nearly 50 N, the tensegrity structure reaches its maximally flattened configuration, storing the greatest amount of elastic energy. Upon releasing the actuator cable tension, the structure transitions back to its rest configuration,

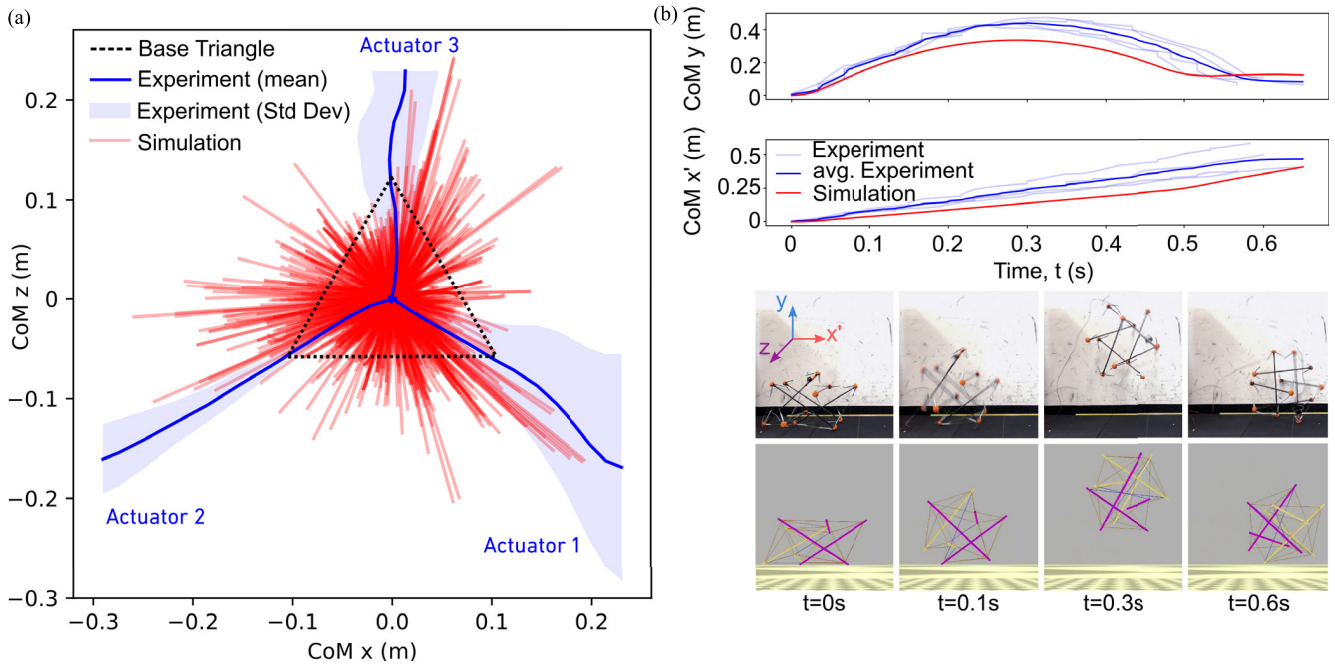

FIGURE 4. Directional jumping characterization. (a) Directional jumping workspace generated in simulation (red), with experimental trajectories superimposed atop in blue. The experimental trajectories correspond to tensioning a single actuator cable to a 50% reduction in length. Experimental trajectories are smoothed (as described in Appendix H in the supplementary material) and averaged across four trials, with the mean plotted in blue and one standard deviation error band in pale blue. These single-actuator jumps are the longest. All other intermediate jumping directions are accessed by superimposing different levels of tensions from the three actuators, demonstrating a large directional workspace accessible by multiactuator jumps. (b) Comparison between simulation and experiments for four directional jumps utilizing one actuator tensioning a cable to 50% length reduction. Note that x' is distinct from x in the coordinate system of A.

generating a resultant force vector orthogonal to the ground, and producing the highest vertical jump recorded at 1.18 m (1.93 BL; Table 1). This height surpasses the state of the art by 9.60× m/m (1.97× BL/BL) [10].

Simulations generally reflect the jumping height trend seen in experiments [Fig. 3(b)]. For the particular case of a 40% reduction in cable length, we note a large standard deviation on the experimental data point, suggesting that near this point the jump height is very sensitive to small variations in global compression. Simulations also indicate this uncertainty; oscillations in predicted jump height occur after a reduction in cable length exceeds 40%. The steep gradients of the simulated curve past 40% reduction in cable length indicate a regime in which such sensitivity would be expected.

We noticed that, when vertically jumping, the tensegrity rotates about the axis of the jump direction, which we attribute to small torques about the structure's center of mass generated by the transition from the flat configuration to the rest configuration. Such a rotation indicates that not all of the stored elastic energy is effectively directed vertically during a jump. Thus, we conducted further jumping tests at maximum cable tension while recording the ballistic trajectory of the robot's center of mass with 3-D motion capture (OptiTrack motion capture system). Simulation trajectories mirror the behavior of the actual robot [Fig. 3(c)], with a mean square error (mse) of $3.0e^{-3}$ m^2 in the y-direction and $2.3e^{-4}$ m^2 in the x-direction. Both simulated and experimental results demonstrate that the robot's horizontal motion is highly sensitive to the timing of actuator release. Even slight asynchrony on the order of 0.1 s during vertical jumps can cause unintended horizontal displacement. This effect arises from the uneven force applied to the ground when the first actuator releases, as well as the influence of subsequent actuator releases while the robot is airborne.

B. DIRECTIONAL JUMPING

For directional jumps, there are options to tension any of the three actuator cables individually or in combinations thereof. To understand the directional steerability of the robot, first, a workspace was generated with NTRT by performing a parameter sweep on each of the three actuator cable length reductions. Namely, we evaluated 1131 parameter sets (generated via the 3-D Cartesian product of the set of actuator cable length reductions {0%, 5%, 10%, 15%, 20%, 25%, 30%, 35%, 40%, 45%, 50%}). We calculated the trajectory of the robot during the jumps by extracting its CoM from slow-motion footage and projecting it onto the plane that the robot was initially at rest on with its down-face (x–z).

The simulated workspace generation demonstrates that the tensegrity robot possesses nearly omnidirectional jumping capability [Fig. 4(a)]. The longest jumps occur along ''principal directions'' and are achieved by tensioning a single actuator cable to 50% length reduction. We corroborated this

TABLE 1. Jumping performance of the robot. Each datapoint created from four samples. "Distance" refers to how far the robot's CoM travels when projected onto the horizontal plane.

Jump	**Avg (m)**	Min (m)	Max (m)	Std Dev (m)
Vertical Jump, Height	**1.09 (1.79BL)**	1.05 (1.73BL)	1.18 (1.93BL)	0.0589 (0.0966BL)
Vertical Jump, Distance	**0.110 (0.180BL)**	0.0361 (0.592BL)	0.280 (0.460BL)	0.113 (0.185BL)
Directional Jump, Height	**0.447 (0.733BL)**	0.423 (0.693BL)	0.475 (0.779BL)	0.0226 (0.0370BL)
Directional Jump, Distance	**0.462 (0.757BL)**	0.353 (0.579BL)	0.589 (0.966BL)	0.106 (0.174BL)

finding through hardware experiments, as indicated by the averaged blue trajectory in the figure. Experimental trajectories differed somewhat from simulated ones. The different trajectory lengths are likely due to the simplified physics of frictional contacts simulation, a model that does not fully capture node endcap slippage of the tensegrity while jumping. Given these unmodeled dynamics, we were deliberately conservative with frictional losses in simulation. We attribute the fact that the experimental trajectories are less straight than those in the simulation to measurement noise during experiments.

Interestingly, attainable jump distance varies as a function of jump direction, rendering an asymmetric workspace. Investigating the cause of this asymmetry led to the discovery that the robot's support surface shifts before a jump, despite the fact that it always starts from the same down-facing position. The shift arises because tensioning different actuators alters the robot's structure, shifting its center of mass, and allowing it to settle into a stable configuration on a transiently formed support face. This transient support face does not correspond to one of the original icosahedral faces but ultimately has bearing on the robot's jumping direction.

An unusual effect of the creation of such transient faces before jumping is that neighboring trajectories in the workspace may not necessarily share similar tensioning patterns. For instance, applying tensions of (0%, 5%, 10%) to three actuators does not produce a trajectory closely aligned with that of (5%, 5%, 10%); they end up being nearly 30° deviated from one another.

To ascertain the effects of differing actuator tensions on the physical robot, we conducted additional directional jump tests with a reduction in actuator cable lengths of 40% and 50%. Reductions below 40% produced minimal jumps, so these were not thoroughly evaluated. Beyond 50% length reduction of one actuator cable, the structure started experiencing self-intersections of the struts.

As predicted by simulation (see Appendix C in the supplementary material), the distance of the jumps using a single actuator increased with increasing actuator cable tension. The maximum distance jump achieved with hardware was 0.59 m (0.97 BL), and used a single actuator at 50% length reduction. Quantifying the trajectory disparity between the simulated and experimental jumps at 50% length reduction gives an mse of $6.4e^{-3}$ m^2 in the y-direction and $9.4e^{-3}$ m^2 in the x-direction [Fig. 4(b)], attesting to the accuracy of the simulation in predicting directional jumps.

In summary, we found that tensioning only one cable approximately aligns the jump direction of the robot with the axis of that tensioned actuator cable. Thus, three principal directions utilize one actuator to jump, separated by approximately 120° in the plane of the downface the robot is resting on. More complex asymmetric actuation strategies involving partial tensioning of the different actuators can elicit higher resolution in jump direction, although there is a nonlinear relationship between actuator tension mappings and jump direction, and self-intersections make actuator cable length reductions past 50% impossible on the physical robot. As a result, steerability is best with single actuator directional jumps. In addition, since using multiple actuators renders transient support faces, control strategies to ensure desired jumping behavior become much more complex. An overview of all jumping results achieved on the actual robot is tabulated in Table 1.

C. JUMPING IN LOWER GRAVITY

A major advantage of the robot is that jumping becomes even more effective in lower gravity. While all hardware experiments were carried out in Earth's gravity of 9.81 ms^{-2}, in simulation we extended these results to low gravity environments, which yielded significantly longer and higher jumps. In Moon gravity, for example, we observed that the robot's workspace could be increased by a distance of 4.6× in the xz-plane [i.e., the same coordinate system as Fig. 4(a)] and 3× vertically. A complete comparison of performance improvements under low gravity can be seen in Appendix F in the supplementary material.

D. SELF-RIGHTING VIA PUNCTUATED ROLLING

If the tensegrity robot is not in the correct configuration for a desired jump, actuating it can shift the CoM outside of the support polygon, tipping the robot onto an adjacent face (in principle, engaging in punctuated rolling). Maneuvering to a viable jump face, so-called ''self-righting,'' is a method to unlock configuration-agnostic jumping. Rolls can be chained together across multiple faces until the robot rests on the desired down-face.

Since vertical jumps and directional jumps require different initial down-face configurations, they may also involve different self-righting maneuvers. We conducted simulations of self-righting, in which the robot was spawned on any down-facing and was commanded to transition to a valid jump face through sequential actuation of any of the three cables.

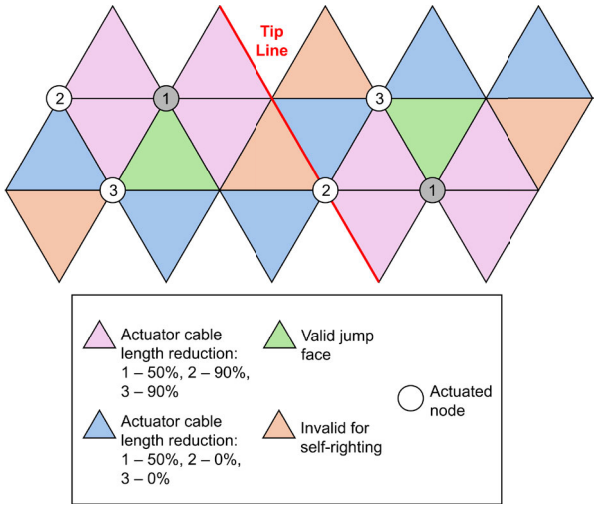

FIGURE 5. Icosahedron net depicting the actuation strategy (on the actual robot) required for self-righting for a directional jump. Here, only the actuator attached to node 1 (gray) is used. The tip line indicates which valid jump face the robot will self-right to—configurations left of the tip line will self-right to the left valid jump face (green), and configurations right of the tip line will self-right to the right valid jump face. Note that for vertical jumps, the required actuation is the same regardless of the face: 46% actuator cable reduction on all actuators.

The results indicated that self-righting would be possible from all down-facing configurations. However, in practice, the simulation does not model the robots' node assemblies that slightly increase the length of their struts. When testing self-righting on the hardware, we saw that structural self-intersections make self-righting only possible from 11 of 20 faces.

For the case of a directional jump using a single actuator on flat terrain—the longest achievable directional jump—the net of the icosahedron illustrates necessary transitions for self-righting (Fig. 5). Although there are invalid faces for achieving directional jumps in any desired direction, it is possible that performing a high vertical jump and tumbling can "reset" the configuration, making it possible to subsequently transition to a face for self-righting.

As another note, we have highlighted the transition mapping for a single actuator jump because it is the longest jump that is possible. There is, however, a distinct map for every individual actuated node. For example, jumps employing only actuators on node 2 or 3 would change the map, as would superposing different cable tensions. Another confounding factor is the nature of the terrain the robot is locomoting on. There are likely unique transition maps for any given terrain profile, where friction and various surface profiles all influence the self-righting of the robot.

E. FREE-FALL IMPACT RESISTANCE

Observations of the robot's behavior during free fall reveal distinct landing orientations based on the alignment of its struts at impact. These orientations can be classified into two main cases: one where the struts are orthogonal to the ground and another where they are angled (see Supplementary Video for examples). The latter is preferable, as it effectively distributes impact energy throughout the tensegrity structure. The former is unfavorable as large forces applied axially to the struts increase the risk of buckling as a structural failure mode.

To assess how different orientations of the tensegrity at impact influence the robot's impact resistance, six free-fall experiments were conducted with drop heights of 4.9 m (8.0 BL), culminating in impact velocities on concrete of 8.7 m/s (14.3 BL/s). We were able to induce a variety of impact orientations during these tests by varying the orientation at release. Surprisingly, the robot did not sustain any damage. We thus moved on to perform three sequential drop tests from the top of a building at 21.5 m (35.2 BL) [Fig. 1(c)].

At these greater heights, the robot achieved velocities of 22.4 ms^{-1} (44.8 BLs^{-1}), and dissipated as much as 102J of energy on impact (where energy dissipated is proportional $mg(h_1 - h_2)$ given the robot's mass m, gravity g, initial drop height h_1, and height of the first bounce h_2). The robot sustained damage to one actuator on the third impact (Supplemental Video shows slow motion recording), limiting its ability to carry out vertical jumps and self-right.

When dropped from greater heights, the robot's slight weight asymmetry caused it to orient itself with the actuators facing downward. This occurred because the actuators on the structure locally increase mass and contribute more to rotational inertia, making it more likely to swing downward during free fall. Despite these high-energy impacts, the tensegrity structure itself remained completely undamaged throughout all drop tests, highlighting its potential as a next-generation space exploration rover capable of withstanding extreme conditions.

F. SHAPE CHANGING

Previous studies on jumping and self-righting elucidated that the robot's form changes significantly during actuation. We use the tightest bounding ellipsoid as a volume metric to compare different deformed configurations. In the robot's rest configuration, this bounding ellipsoid is just a sphere, so we define one BL to be the diameter of this sphere (0.61 m). This metric yields a rest volume of 0.119 m^3. When in the fully compressed, flattened configuration, the robot's bounding ellipsoid has a volume of 0.0293 m^3, meaning that a volume reduction in excess of 4× is possible without inflicting any damage. Flattening the robot into a disk [Fig. 1(a)], or converting it to a rhombohedron-like shape [Fig. 1(b)] could prove useful for transport. No damage was observed in any compressed configuration, suggesting that with the skew-central actuation topology, the directional jumping tensegrity can be readily stowed and transported in a spacecraft.

IV. FIELD TESTING

To assess the robot in a more realistic planetary environment and to validate the results seen in the lab, the

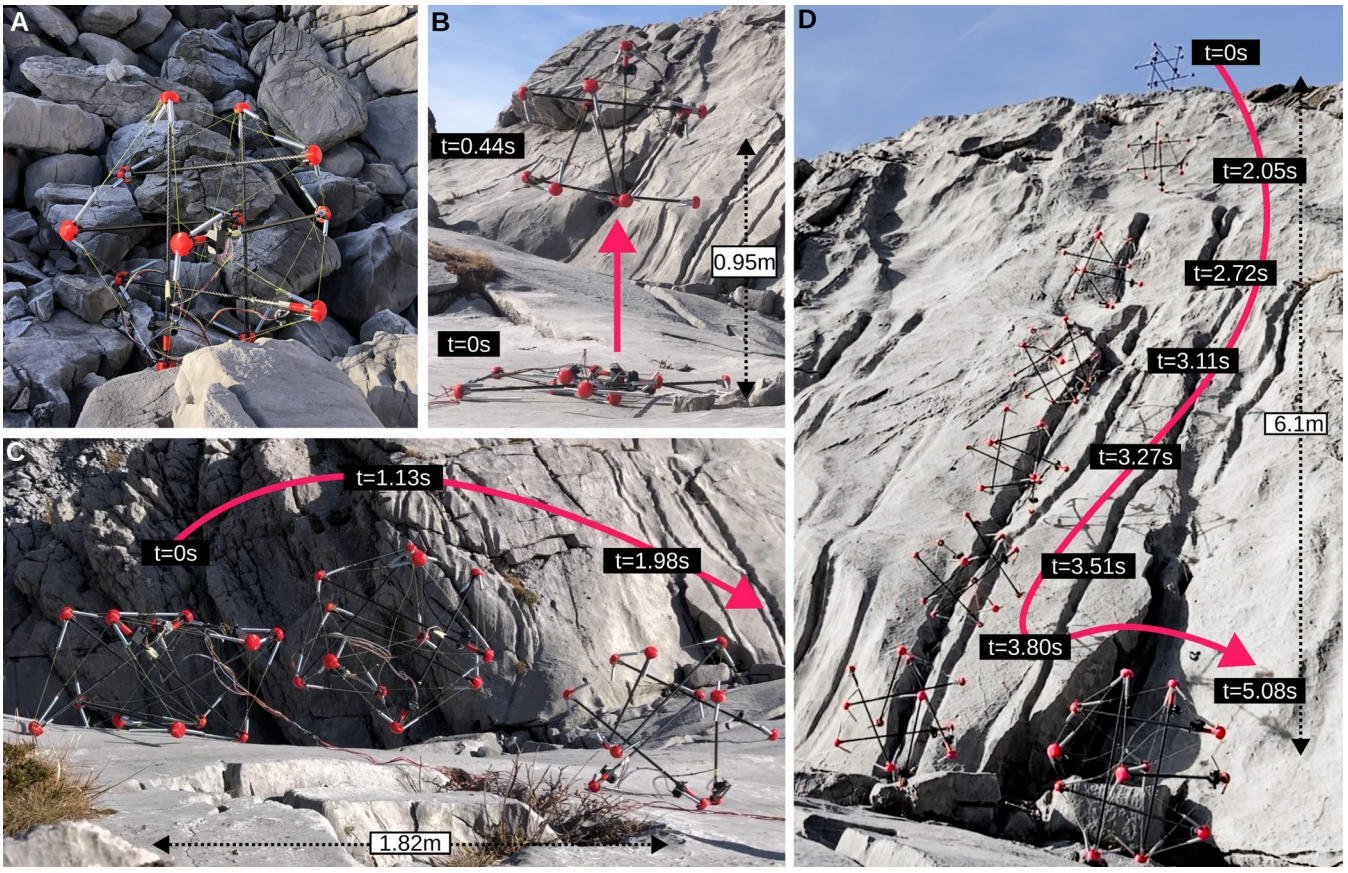

FIGURE 6. Field testing. (a) High-jumping tensegrity robot in the mountain terrain environment. (b) High jumping is still successful even with the undulations and variable friction of the rocky ground. However, the maximum attainable height is impacted. (c) Directional jumping enables traversal of long distances, especially when the robot subsequently tumbles down slight declines. (d) Tensegrity robot retains functionality after the impacts of rolling off a 6.1-m-tall (10.0 BL) cliff face.

robot was deployed at the foot of Säntis, a mountain in the Appenzell Alps of eastern Switzerland (Fig. 6(a); Supplementary Video). The environment, largely devoid of vegetation, features rugged rocky terrain, including shale, scree, and boulders at scales many times the robot's BL.

Both vertical and directional jump motion primitives were assessed in this mountainous environment [Fig. 6(b) and (c)]. Undulations, the presence of loose rocks and particulates, and the grade of the rock face the robot was situated on influenced the robot's jumping performance. For instance, we noted that the maximum height achieved by the vertical jumps was reduced because of local variations in terrain, and thereby the robot's inability to generate productive thrust uniformly during a jump. Thus, the robot was only able to reach a height that was 80% of the maximum attained in the lab. An additional constraint imposed by the complex environment was that the combined slackness and motion induced in the structural cables during compression could occasionally cause a cable to become entangled on a nearby object, interfering with jumping. On the other hand, we noted that even shallow declines facilitated significant rolling after directional jumps, increasing the robot's range.

Several drop tests were conducted in the field to ascertain the durability of the robot in such a challenging operational environment. Even when dropped from cliffs as tall as 6.1 m (10.0 BL), the robot did not sustain any damage that impeded its locomotion capabilities [Fig. 6(d)]. The only damage observed was slight wear on the 3-D-printed endcaps after three sequential falls from the cliff face. Notably, the robot builds up substantial momentum during these falls, exhibiting a unique tumbling direction each time we release it.

V. DISCUSSION AND CONCLUSION

Through first-principles analysis, numerical simulations, and experimental validation in both laboratory and field environments, this work demonstrated the potential of a high-jumping tensegrity robot employing clutch-based actuators and a newly introduced skew-centric actuation topology. The robot achieved vertical jumps of 1.18 m (1.93 BL), controlled directional jumps up to 0.59 m (0.97 BL), and quasistatic self-righting from 11 of 20 possible initial down-face configurations. The robot also exhibited remarkable durability, surviving free-fall drops of 21.5 m (35.2 BL) onto concrete and tumbling drops over 6.1 m (10 BL) in rugged terrain with minimal damage. Additionally, it demonstrated

the ability to reduce its volume by more than four times without structural damage. Jumping mechanics were generally well-recapitulated by the NTRT simulation tool, indicating potential for further development of jumping and locomotion control strategies.

Through the tests with the robot, we also learned valuable lessons about the mechanics and design of jumping tensegrity systems. A key learning is the importance of synchrony in the actuator release for achieving vertical jumping. Without synchronized actuator release, additional momentum imparted by releasing actuators in the air serves to deviate the ballistic trajectory from vertical. Although counterproductive for vertical jumping, this asynchronous release could actually be leveraged to control the robot mid-air in future work.

Another useful finding is the role of transient support faces during actuator pretensioning before directional jumps. These virtual faces are rendered as a function of tension and terrain characteristics, do not correspond to the robot's original icosahedral structure, and complicate targeting a specific jump direction. Investigating the relationship between these virtual faces, different tensegrity topologies, and control strategies thus constitutes a rich future research direction.

Additionally, while the skew-centric actuation topology presented herein was designed for simplicity and to steer jumps through superposition of three actuator tensions (as it effectively forms a basis in 3-D), self-righting experiments revealed a limitation: the three-actuator configuration does not always permit self-righting to a viable down-face. Including more centrally spanning actuated cables could enhance self-righting capabilities and even alleviate the need to self-right altogether by making it possible to jump from any orientation. Adding actuators to the robot in this fashion would pose tradeoffs in terms of mass and resilience to fall damage and merits systemic analysis. Alternate actuator configurations may also create a larger internal volume for a payload, although the positioning of this payload must be carefully considered as its deceleration volume during impact varies with orientation, as noted in [2]. Hardware demonstrations of directional jumps were constrained to those using a single actuator in the present analysis, but a more versatile actuation strategy may also permit a comprehensive investigation of multiactuator directional jumping.

Finally, field tests highlighted challenges with respect to the variability of jumping height and direction on uneven terrain. Field tests, by the same token, showcased emergent properties of the platform not seen in the structured lab environment: the ability to overcome obstacles, tumble over cliff faces, and leverage declines to increase the distance traveled by a single jump.

Overall, this work serves as a proof-of-concept for tensegrities' potential for controlled directional jumping, leveraging their own structures. The steerable high-jumping tensegrity robot herein has the potential to clear a range of obstacles, mitigate orientation dependence, and improve impact resistance of next-generation space rovers, in comparison to conventional wheeled or legged platforms. Through the use of simple actuation strategies, directional high-jumping tensegrities could one day be deployed far from Earth amid treacherous planetary terrains.

REFERENCES

[1] *Overview of Materials for Epoxy/Carbon Fiber Composite*. Accessed: Jun. 22, 2024. [Online]. Available: https://www.matweb.com/search/datasheetprint.aspx?matguid=39e40851fc164b6c9bda29d798bf3726

[2] V. SunSpiral, A. Agogino, and D. Atkinson, "Super ball bot-structures for planetary landing and exploration, NIAC phase 2 final report," 2015.

[3] N. Amir, M. S. M. Hisham, and K. A. Z. Abidin, "Study of physical properties and shock absorption abilities of starch polymer foam as cushioning material for packaging," in *Proc. MATEC Web Conf.*, vol. 225, 2018, p. 06010.

[4] P. Arm et al., "Scientific exploration of challenging planetary analog environments with a team of legged robots," *Sci. Robot.*, vol. 8, no. 80, Jul. 2023, Art. no. eade9548.

[5] J. Bruce, K. Caluwaerts, A. Iscen, A. P. Sabelhaus, and V. SunSpiral, "Design and evolution of a modular tensegrity robot platform," in *Proc. IEEE Int. Conf. Robot. Autom. (ICRA)*, May 2014, pp. 3483–3489.

[6] R. G. Budynas and J. K. Nisbett, *Shigley's Mechanical Engineering Design*, vol. 9. New York, NY, USA: McGraw-Hill, 2011.

[7] K. Chang, "Moon lander is lying on its side but still functional, officials say," The New York Times, New York, NY, USA, Tech. Rep., Feb. 2024.

[8] L.-H. Chen et al., "Inclined surface locomotion strategies for spherical tensegrity robots," in *Proc. IEEE/RSJ Int. Conf. Intell. Robots Syst. (IROS)*, Sep. 2017, pp. 4976–4981.

[9] M. Chen and R. E. Skelton, "A general approach to minimal mass tensegrity," *Composite Struct.*, vol. 248, Sep. 2020, Art. no. 112454.

[10] Y. S. Chung, J.-H. Lee, J. H. Jang, H. R. Choi, and H. Rodrigue, "Jumping tensegrity robot based on torsionally prestrained SMA springs," *ACS Appl. Mater. Interfaces*, vol. 11, no. 43, pp. 40793–40799, Oct. 2019.

[11] J. Friesen, A. Pogue, T. Bewley, M. de Oliveira, R. Skelton, and V. Sunspiral, "DuCTT: A tensegrity robot for exploring duct systems," in *Proc. IEEE Int. Conf. Robot. Autom. (ICRA)*, May 2014, pp. 4222–4228.

[12] Y. Gao and S. Chien, "Review on space robotics: Toward top-level science through space exploration," *Sci. Robot.*, vol. 2, no. 7, Jun. 2017, Art. no. eaan5074.

[13] K. Garanger et al., "Soft tensegrity systems for planetary landing and exploration," *Earth Space*, vol. 2021, pp. 841–854, Apr. 2021.

[14] E. Gibney, "Israeli spacecraft beresheet crashes into the moon," *Nature*, vol. 568, no. 7752, pp. 286–287, Apr. 2019.

[15] T. D. Glotch et al., "The scientific value of a sustained exploration program at the Aristarchus Plateau," *Planet. Sci. J.*, vol. 2, no. 4, p. 136, Jul. 2021.

[16] M. P. Golombek et al., "Rock size-frequency distributions on Mars and implications for Mars exploration rover landing safety and operations," *J. Geophys. Res., Planets*, vol. 108, no. E12, pp. 1–23, Dec. 2003.

[17] J. Jeong et al., "Spikebot: A multigait tensegrity robot with linearly extending struts," *Soft Robot.*, vol. 11, no. 2, pp. 207–217, Apr. 2024.

[18] G.-P. Jung et al., "JumpRoACH: A trajectory-adjustable integrated jumping–crawling robot," *IEEE/ASME Trans. Mechatronics*, vol. 24, no. 3, pp. 947–958, Jun. 2019.

[19] K. Kim et al., "Hopping and rolling locomotion with spherical tensegrity robots," in *Proc. IEEE/RSJ Int. Conf. Intell. Robots Syst. (IROS)*, Oct. 2016, pp. 4369–4376.

[20] S. Lessard et al., "A bio-inspired tensegrity manipulator with multi-DOF, structurally compliant joints," in *Proc. IEEE/RSJ Int. Conf. Intell. Robots Syst. (IROS)*, Oct. 2016, pp. 5515–5520.

[21] T. D. J. Mateo Sanguino, "50 years of rovers for planetary exploration: A retrospective review for future directions," *Robot. Auto. Syst.*, vol. 94, pp. 172–185, Aug. 2017.

[22] S. Mintchev, D. Zappetti, J. Willemin, and D. Floreano, "A soft robot for random exploration of terrestrial environments," in *Proc. IEEE Int. Conf. Robot. Autom. (ICRA)*, May 2018, pp. 7492–7497.

[23] B. T. Mirletz, I.-W. Park, R. D. Quinn, and V. SunSpiral, "Towards bridging the reality gap between tensegrity simulation and robotic hardware," in *Proc. IEEE/RSJ Int. Conf. Intell. Robots Syst. (IROS)*, Sep. 2015, pp. 5357–5363.

[24] R. Motro, *Tensegrity: Structural Systems for the Future*. Amsterdam, The Netherlands: Elsevier, 2003.

[25] R. P. Mueller and P. J. van Susante, "A review of extra-terrestrial mining robot concepts," in *Earth and Space 2012: Engineering, Science, Construction, and Operations in Challenging Environments*, 2012, pp. 295–314.
[26] C. Paul, F. J. Valero-Cuevas, and H. Lipson, "Design and control of tensegrity robots for locomotion," *IEEE Trans. Robot.*, vol. 22, no. 5, pp. 944–957, Oct. 2006.
[27] H. Peng, H. Yang, F. Li, C. Yang, and N. Song, "A unified framework for mechanical modeling and control of tensegrity robots," *Mechanism Mach. Theory*, vol. 191, Jan. 2024, Art. no. 105498.
[28] S. Savin, A. Al Badr, D. Devitt, R. Fedorenko, and A. Klimchik, "Mixed-integer-based path and morphing planning for a tensegrity drone," *Appl. Sci.*, vol. 12, no. 11, p. 5588, May 2022.
[29] D. S. Shah et al., "Tensegrity robotics," *Soft Robot.*, vol. 9, no. 4, pp. 639–656, Aug. 2022.
[30] Z. Shiller, "Obstacle traversal for space exploration," in *Proc. ICRA. Millennium Conf., IEEE Int. Conf. Robot. Autom. Symposia*, vol. 2, Jun. 2000, pp. 989–994.
[31] R. E. Skelton, R. Adhikari, J.-P. Pinaud, W. Chan, and J. W. Helton, "An introduction to the mechanics of tensegrity structures," in *Proc. 40th IEEE Conf. Decis. Control*, vol. 5, Dec. 2001, pp. 4254–4259.
[32] P. D. Spudis, B. Bussey, J. Plescia, J.-L. Josset, and S. Beauvivre, "Geology of Shackleton Crater and the south pole of the moon," *Geophys. Res. Lett.*, vol. 35, no. 14, pp. 1–5, Jul. 2008.
[33] *Hollow Circle (Annulus)*. Accessed: Jun. 23, 2024. [Online]. Available: https://structx.com/ShapeFormulas014.html
[34] D. Surovik, K. Wang, M. Vespignani, J. Bruce, and K. E. Bekris, "Adaptive tensegrity locomotion: Controlling a compliant icosahedron with symmetry-reduced reinforcement learning," *Int. J. Robot. Res.*, vol. 40, no. 1, pp. 375–396, Jan. 2021.
[35] G. Thomas and V. V. Vantsevich, "Wheel-terrain-obstacle interaction in vehicle mobility analysis," *Vehicle Syst. Dyn.*, vol. 48, no. sup1, pp. 139–156, Dec. 2010.
[36] B. R. Tietz, R. W. Carnahan, R. J. Bachmann, R. D. Quinn, and V. SunSpiral, "Tetraspine: Robust terrain handling on a tensegrity robot using central pattern generators," in *Proc. IEEE/ASME Int. Conf. Adv. Intell. Mechatronics*, Jul. 2013, pp. 261–267.
[37] B. Trimmer, "An interview with NASA principal investigator vytas SunSpiral: Expert opinion on the advantages and limitations of soft robotics," *Soft Robot.*, vol. 2, no. 2, pp. 51–58, Jun. 2015.
[38] M. Vespignani, C. Ercolani, J. M. Friesen, and J. Bruce, "Steerable locomotion controller for six-strut icosahedral tensegrity robots," in *Proc. IEEE/RSJ Int. Conf. Intell. Robots Syst. (IROS)*, Oct. 2018, pp. 2886–2892.
[39] M. Vespignani, J. M. Friesen, V. SunSpiral, and J. Bruce, "Design of SUPERball v2, a compliant tensegrity robot for absorbing large impacts," in *Proc. IEEE/RSJ Int. Conf. Intell. Robots Syst. (IROS)*, Oct. 2018, pp. 2865–2871.
[40] M. Zhang et al., "Deep reinforcement learning for tensegrity robot locomotion," in *Proc. IEEE Int. Conf. Robot. Autom. (ICRA)*, May 2017, pp. 634–641.
[41] F. Zhou et al., "Simulations of Mars rover traverses," *J. Field Robot.*, vol. 31, no. 1, pp. 141–160, Jan. 2014.